

Article

A Cyclic Calibration Method of Milling Force Coefficients Considering Elastic Tool Deformation

Chang Yang ¹, Rong Yu ^{1,*} and Shanglei Jiang ²¹ School of Transportation, Inner Mongolia University, Hohhot 010070, China; 32124091@mail.imu.edu.cn² School of Mechanical Engineering, Dalian Jiaotong University, Dalian 116086, China; sljiang@djtu.edu.cn

* Correspondence: yurong@imu.edu.cn

Abstract: In metal-cutting technology, milling plays an important role in the product development cycle. The accurate modeling and prediction of milling forces have always been research hotspots in this field. The mechanical model based on unit-cutting force coefficients has a high prediction accuracy of cutting forces, and it is therefore widely used in the modeling of milling forces. The calibration of the cutting force coefficients can be realized by linear regression analysis of the measured average milling forces, but it needs to carry out multiple groups of variable feed slot milling experiments with full radial depth of cut, and it cannot well represent the interaction condition in peripheral milling with a non-full radial depth of cut. In peripheral milling, the tool will inevitably deform under the influence of cutting force in the direction perpendicular to the machining surface. If the force-induced deformation is ignored, the calibration of the cutting force coefficients will be out of alignment. For this non-slot milling condition where one side of the tool is mainly stressed, a cyclic calibration method for milling force coefficients considering elastic deformation along the axial contact range is proposed. Firstly, the cutting force coefficients are preliminarily calibrated by the experimental data, and, secondly, tool deformation is calculated through a preliminarily calibrated cutting force model cycle until convergence, before cutting boundaries are updated. The cutting force coefficient is then calibrated again, and it is brought back to the cantilever beam model in order to calculate the tool deformation again. The above process is repeated until the cutting force coefficient is convergent. Finally, the cutting force coefficients are obtained in order to predict and model the milling forces.

Keywords: peripheral milling; end milling; tool deformation; cutting force coefficient; modeling of milling forces



Citation: Yang, C.; Yu, R.; Jiang, S. A Cyclic Calibration Method of Milling Force Coefficients Considering Elastic Tool Deformation. *Machines* **2023**, *11*, 821. <https://doi.org/10.3390/machines11080821>

Academic Editor: Angelos P. Markopoulos

Received: 17 July 2023

Revised: 3 August 2023

Accepted: 8 August 2023

Published: 10 August 2023



Copyright: © 2023 by the authors. Licensee MDPI, Basel, Switzerland. This article is an open access article distributed under the terms and conditions of the Creative Commons Attribution (CC BY) license (<https://creativecommons.org/licenses/by/4.0/>).

1. Introduction

CNC milling technology is an advanced machining technology, especially for complex curved parts. Among milling techniques, peripheral milling can achieve high-quality surface treatments with a fast material removal rate, so it is widely employed in various scenarios. For example, peripheral milling can be used for contouring and profiling operations, which allows for the precise removal of material from the periphery of the workpiece in order to achieve the desired shape, such as the machining of an impeller. It is of great significance to study the mechanics of the peripheral milling process in order to control the machining quality and to improve machining efficiency [1].

There are many types of high-performance materials and many machining parameters, and most of the previous research on cutting and machining is based on empirical analysis. The deformation and bounce of tools and parts is caused by cutting forces, and the actual machined surface of the part will thus have a large deviation from the target value [2]. Consequently, technicians are usually forced to use smaller cutting amounts and repeat finishing operations to ensure the machining accuracy of the part, which inevitably results in a waste of resources. The use of a cutting force prediction model can carry out cutting force simulation experiments under different conditions, providing theoretical support

for optimizing machining parameters, simulating cutting system vibration, monitoring tool wear, conducting machining error analysis, and others [3]. Therefore, it is necessary and meaningful to simulate the machining process by establishing an accurate model for predicting cutting force, simulating the deformation law of the cutting process of the tool and the workpiece, and then selecting the appropriate cutting parameters to improve machining accuracy and machining efficiency.

The modeling methods for cutting machining can generally be divided into four categories: empirical methods, analytical methods, finite element methods, and mechanical methods. Mechanical modeling methods are the most widely used due to their advantages of simple models and better prediction accuracy under a wider range of cutting conditions [4], and scholars have conducted an in-depth exploration of cutting force modeling methods [5]. There are several existing approaches to modeling cutting forces: early fully empirical models based on experimental data, physical models based on cutting mechanisms and material intrinsic relationships, mechanical models based on unit cutting force coefficients, and neural network models based on artificial intelligence [6]. Among these, mechanical models based on unit cutting force coefficients, which allow the cutting force at any machining instant to be determined concisely and effectively based on the area of the trace element load at the cutting edge and the unit cutting force coefficients [7], have been widely studied and applied.

Compared to mechanical methods, the mechanical model based on the unit cutting force coefficient allows the cutting force for an arbitrary machining instant to be determined concisely and efficiently from the micro-element loading area of the cutting edge and the unit cutting force coefficient, and it can thus be used well for more complex tool designs [8]. Kao et al. [9] proposed a method for calculating the cutting force coefficients of a ball-end milling machine based on the average cutting forces and parameters, such as tool geometry and cutting conditions. Wang et al. [10] found that the cutting force coefficients are only related to the workpiece material and tool geometry parameters, and that they are not affected by the milling parameters. Guo et al. [11] developed an instantaneous undeformed cut thickness (IUCT) model using error compensation theory combined with the true trajectory of the tool edge, and they calculated the cutting force coefficients using the average IUCT. Kao et al. [12] developed a linear forces model incorporating the tool helix angle to calculate the cutting force coefficients based on the average cutting forces and tool geometry. Liu et al. [13] used an inverse filter dynamic compensation technique to eliminate the influence of the dynamic characteristics of the test system and high-frequency noise on the signals of the cutting forces, and the dynamic compensation experimental measurements were followed by the average forces method for cutting force coefficient calibration. Unlike the general average milling forces calibration method based on slot milling experiments, Gradisek et al. [14] proposed a cutting force coefficients calibration method that can be used under arbitrary radial immersion conditions, making the calibration results more accurate.

This paper considers the effect of tool deformation induced by radial cutting forces on the starting and exist angles of the tool during the cutting process, using the cantilever beam model to cyclic iterative calculation the tool micro-element deformation to approximate the true tool deformation, and then the starting and exist angles are recalculated and the cutting boundary is modified. The cutting force coefficients are cyclically calibrated until convergence, and they are then developed as a predictive model for peripheral milling cutting forces considering tool deformation. Simulating the milling forces at the same time, milling tests are carried out under the same conditions. Verifying the accuracy of the cutting forces prediction model considering tool deformation, the simulation results indicate that the milling force prediction model is very accurate and that the coefficients calibrated are accurate. The most prominent method in this field is the calibration method based on the average force of slot milling, but the calibration of the coefficients taking into account the tool's real deformation has not yet had a lot of work conducted on it, and based on the method proposed in this paper, the obtained coefficients are more representative of the real role of the metal in the cutting process of those several deformation zones. This

is also of practical significance for the consideration of the deformation of the machining stability of the prediction.

2. Cyclic Calibration of Peripheral Milling Cutting Force Coefficients Considering Tool Deformation

2.1. Calibration of Cutting Force Coefficients for Arbitrary Immersion Angles

The coefficient calibration method used by the general model is to calibrate the coefficients through slot milling experiments. The coefficient calibration method used in this paper can calibrate the cutting force coefficients for milling experiments under arbitrary immersion conditions, and the coefficient calibration results will be closer to the real values. The relationship between the average milling forces and the cutting force coefficients is shown in Equation (1):

$$\begin{bmatrix} \overline{F_x} \\ \overline{F_y} \\ \overline{F_z} \end{bmatrix} = \frac{f_t}{\varphi} \begin{bmatrix} C_3A_1 & (C_2 - C_1)A_2 & (C_2 - C_1)A_3 \\ -(C_2 - C_1)A_1 & C_3A_2 & C_3A_3 \\ 0 & -C_5A_3 & C_5A_2 \end{bmatrix} \times \begin{bmatrix} K_{tc} \\ K_{nc} \\ K_{ac} \end{bmatrix} + \frac{1}{\varphi} \begin{bmatrix} -C_4B_1 & C_5B_2 & C_5B_3 \\ -C_5B_1 & -C_4B_2 & -C_4B_3 \\ 0 & 2C_1B_3 & -2C_1B_2 \end{bmatrix} \times \begin{bmatrix} K_{te} \\ K_{ne} \\ K_{ae} \end{bmatrix} \quad (1)$$

where the geometric constants A and B represent the influence of cutter geometry on the average cutting and edge forces, respectively, and the immersion constants C contain the terms depending on the immersion angles (see Appendix A).

The names, meanings, and units of each parameter in the formula are shown in Table 1:

Table 1. Formula Symbol Table.

Symbol	Significance	Unit	Symbol	Significance	Unit
$\overline{F_{\bullet}}$	The average milling forces for each direction	N	$\overline{F_{\bullet c}}$	The average cutting forces	N
$\overline{F_{\bullet e}}$	The average edge forces	N	f_t	Tool feed rate per tooth	mm/tooth
E	Young's modulus for tool	GPa	I	The area moment of inertia of the tool	mm ⁴
K_c	Tool clamping stiffness	N/mm	$\delta_{(k)}$	Tool microelement deformation	mm
d & r	Diameter and radius	mm	a	The radial depth of cut	mm
b	The axial depth of cut	mm	φ	The current rotation angle of the cutting-edge micro-element	degree
φ_s	The tool starting angle	degree	N	The number of tool teeth	

Equation (2) represents the average cutting forces per cutting tooth as a linear function of feed f_t :

$$\overline{F_{\bullet}} = \overline{F_{\bullet c}} f_t + \overline{F_{\bullet e}} \quad (2)$$

The left-hand side of the equation shows the average three-dimensional milling forces. As shown in Figure 1, Equation (2) is expressed as a linear function of the three-dimensional average forces and the tool feed rate, with the average cutting forces and the average edge forces corresponding to the slope and the intercept of the line, respectively.

The cutting force coefficients and the edge force coefficients can be obtained by combining Equations (1) and (2):

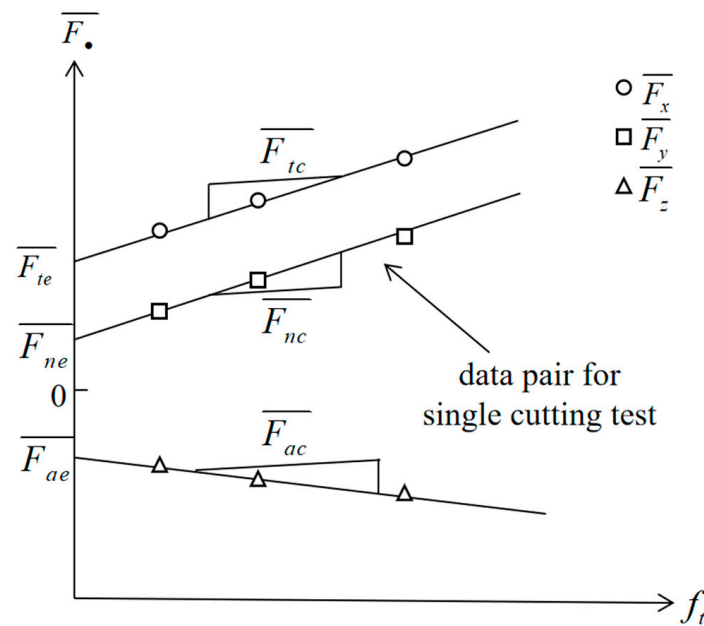


Figure 1. Feed rate versus mean forces.

2.2. Calculation of Tool Deformation Cycles under Static Forces Induction

Under the action of radial cutting forces, the tool will sustain radial deformation, which will inevitably cause the immersion angle of the tool to change. Introducing the cantilever beam model, calculating the radial deformation of the tool based on the radial forces applied to the tool, and then bringing it back to perform a radial forces calculation that takes into account the tool deformation are then performed. There is then iteration until the tool deformation converges, and, at this point, the tool deformation is considered the same as the experimental tool deformation.

Considering the tool as a cantilever beam [15], the end mill structure is modeled as shown in Figure 2, where the tool is divided into equally spaced axial nodes, with each tool micro-element corresponding to a node in the axial direction z. The radial deformation of the tool micro-element is calculated by the radial forces applied to each tool micro-element during milling, and the deformation at node k caused by the forces applied at node h is given by the following equation:

$$\delta_{k,h} = \begin{cases} \frac{\Delta F_{y,h} \mu_h^2}{6EI} (3\mu_h - \mu_k) + \frac{\Delta F_{y,h}}{K_c}, & 0 < \mu_k < \mu_h \\ \frac{\Delta F_{y,h} \mu_h^2}{6EI} (3\mu_k - \mu_h) + \frac{\Delta F_{y,h}}{K_c}, & \mu_h < \mu_k \end{cases} \quad (3)$$

where $\mu_k = l - Z_k$, l is the length from the free end of the tool to the clamping section, and where Z_k denotes the z-axis boundary of the tool at node k. Finally, the total static deformation at nodal station k is calculated by superimposing the deformation generated by all (n + 1) of the nodal forces as follows:

$$\delta_{(k)} = \sum_{h=1}^{n+1} \delta_{k,h} \quad (4)$$

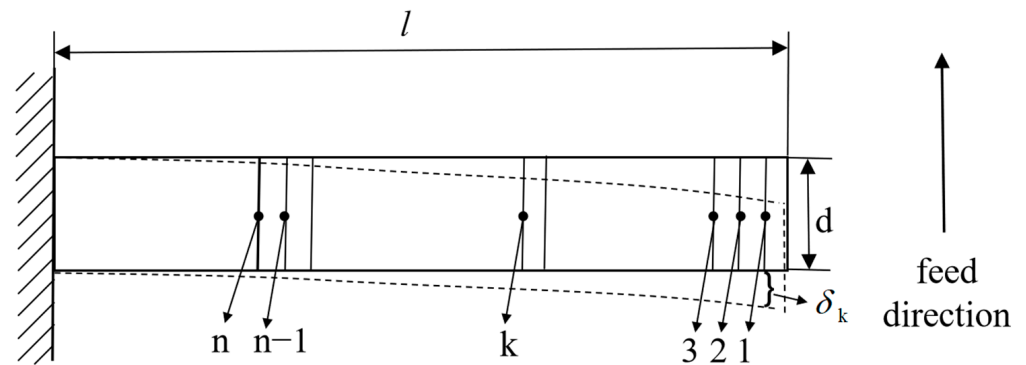


Figure 2. Cantilever beam model and corresponding node of the tool element.

As shown in Figure 3 below, the radial force on the tool from the material causes radial deformation of the tool, each tool micro-element deformation is different, the deformation of the tool end is the largest, and the tool immersion angle is related to the radial depth of cut a and the radial deformation of the micro-element. Considering the tool deformation caused by the radial forces, the tool immersion angle is bound to change, the radial deformation of the tool micro-element of different axial heights is different, and the immersion angle is also different. For different milling methods, the immersion angle is calculated in different ways. The starting angle φ_s for up-milling is 0° , and the exist angle φ_e is shown in the left figure of Figure 3. The exist angle φ_e for down-milling is 180° , and the starting angle φ_s is shown in the right figure of Figure 3. In this paper, the actual depth of cut of each tool micro-element is calculated according to the radial deformation of the tool and the immersion angle, which is recalculated in Equation (5):

$$\begin{aligned} \varphi_{s,k} &= \pi - \arccos\left(\frac{(r - a - \delta_k)}{r}\right) \\ \varphi_{e,k} &= \arccos\left(\frac{(r - a - \delta_k)}{r}\right) \end{aligned} \tag{5}$$

where δ_k is the radial deformation of the k -th tool microelement. $\varphi_{s,k}$ is the calculation method for the up-milling starting angle, and $\varphi_{e,k}$ is the calculation method for the down-milling exist angle.

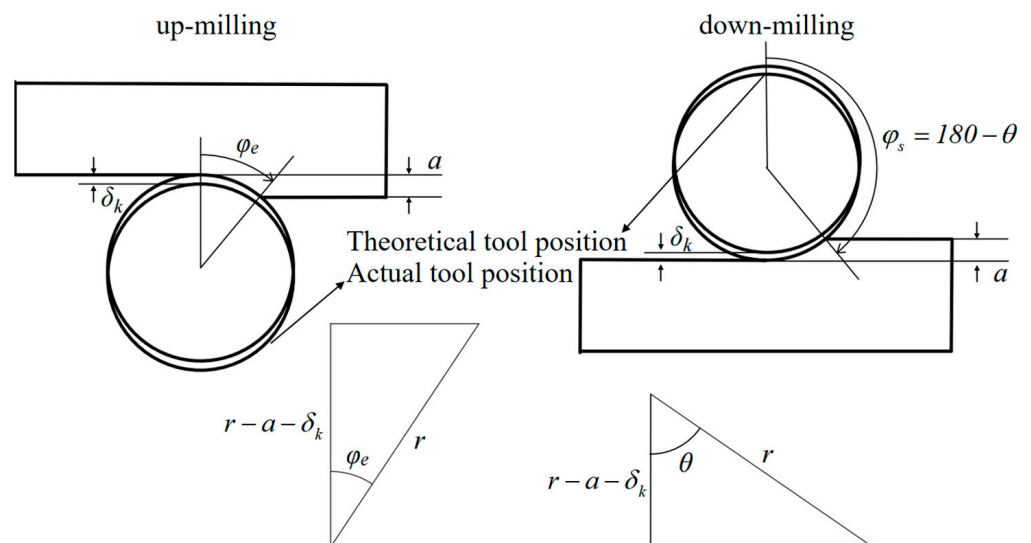


Figure 3. Effect of tool deformation on immersion angle.

2.3. Cyclic Calibration of Cutting Force Coefficients

The calculation of the cutting force coefficients requires the tool immersion angle. This paper improves the calculation accuracy of the cutting force coefficients from the perspective of correcting the cutting boundary in order to improve the prediction accuracy of the milling forces model.

The dual loop algorithm is shown in Algorithm 1 below. Firstly, the cutting force coefficients are initially calibrated based on the experimentally measured three-dimensional milling average forces and the input machining parameters. Secondly, tool deformation calculations are performed under the static force that is induced, and the tool micro-element deformation is calculated according to the radial cutting forces of the model. The immersion angle is then calculated, the cutting forces are recalculated, the tool deformation is calculated with the new cutting forces, the immersion angle is corrected, and the cycle is iterated until the tool radial deformation converges. At this point, the tool deformation is considered to be close to the real value of the actual cutting process under the current milling force coefficients and the immersion angle of each tool micro-element, and the cutting boundary is saved. The cutting boundary is then adjusted, and the cutting force coefficient is calibrated again. If the value of the cutting force coefficient changes, the tool deformation calculation under static force induction is performed again until the calibrated cutting force coefficients converge and the cyclic calibration of the cutting force coefficients is completed, and the tool deformation at this point is saved.

Algorithm 1. Implementation of dual loop calibration.

1. Obtain the values of processing conditions, tools, and other related parameters:
get $\bar{F}_\bullet, f_t, E, K_c, m = 0$, etc.
 2. Preliminary calibration of cutting force coefficients:

$$\bar{F}_\bullet = \bar{F}_c f_t + \bar{F}_e$$

$$K_{\bullet c}^m = f(\varphi_{s,k}^m, \bar{F}_{xc}, \bar{F}_{yc}, \bar{F}_{zc})$$

$$K_{\bullet e}^m = f(\varphi_{s,k}^m, \bar{F}_{xe}, \bar{F}_{ye}, \bar{F}_{ze})$$
 3. Cycle calculation of tool deformation:
 Get $K_{\bullet c}, K_{\bullet e}$
for $n = 1:30$
 Calculate tool element radial force $\Delta F_{y,h}$
 Calculate tool element deformation and update cutting boundaries see Equations (3)–(5)

$$\delta_{(k)} = \sum_{h=1}^{n+1} \delta_{k,h}$$

$$\varphi_{s,k}^{m+1} = \pi - \arccos\left(\frac{(r-a-\delta_k)}{r}\right)$$

$$\varphi_{e,k}^{m+1} = \arccos\left(\frac{(r-a-\delta_k)}{r}\right)$$
if $\delta_{(k)}^{i+1} = \delta_{(k)}^i$ **then**
 break
end
end
 4. Recalibrate the cutting force coefficients:
 update cutting boundaries $\varphi_{s,k}^{m+1}$ or $\varphi_{e,k}^{m+1}$

$$\bar{F}_\bullet = \bar{F}_c f_t + \bar{F}_e$$

$$K_{\bullet c}^{m+1} = f(\varphi_{s,k}^{m+1}, \bar{F}_{xc}, \bar{F}_{yc}, \bar{F}_{zc})$$

$$K_{\bullet e}^{m+1} = f(\varphi_{s,k}^{m+1}, \bar{F}_{xe}, \bar{F}_{ye}, \bar{F}_{ze})$$
if $K_{\bullet c}^{m+1} = K_{\bullet c}^m$ & $K_{\bullet e}^{m+1} = K_{\bullet e}^m$ **then**
 output $K_{\bullet c}, \delta_{(k)}$
else
 $m = m + 1$
 go to 3;
end if
 5. Return computed values:
 return $K_{\bullet c}, \delta_{(k)}^i$
-

3. Peripheral Milling Cutting Forces Modeling Considering Static Force-Induced Deformation

Based on the obtained cutting force coefficients, a peripheral milling cutting forces model considering the static force-induced deformation is established, in which the tool is sliced and differentiated along the axial direction. The cutting process of the whole tool is regarded as the comprehensive action of each tool micro-element, and the instantaneous cutting forces of the tool are obtained by superimposing the instantaneous forces of each tooth of each tool micro-element. The cyclic calibration of cutting force coefficients and the modeling of milling force prediction are shown in Figure 4.

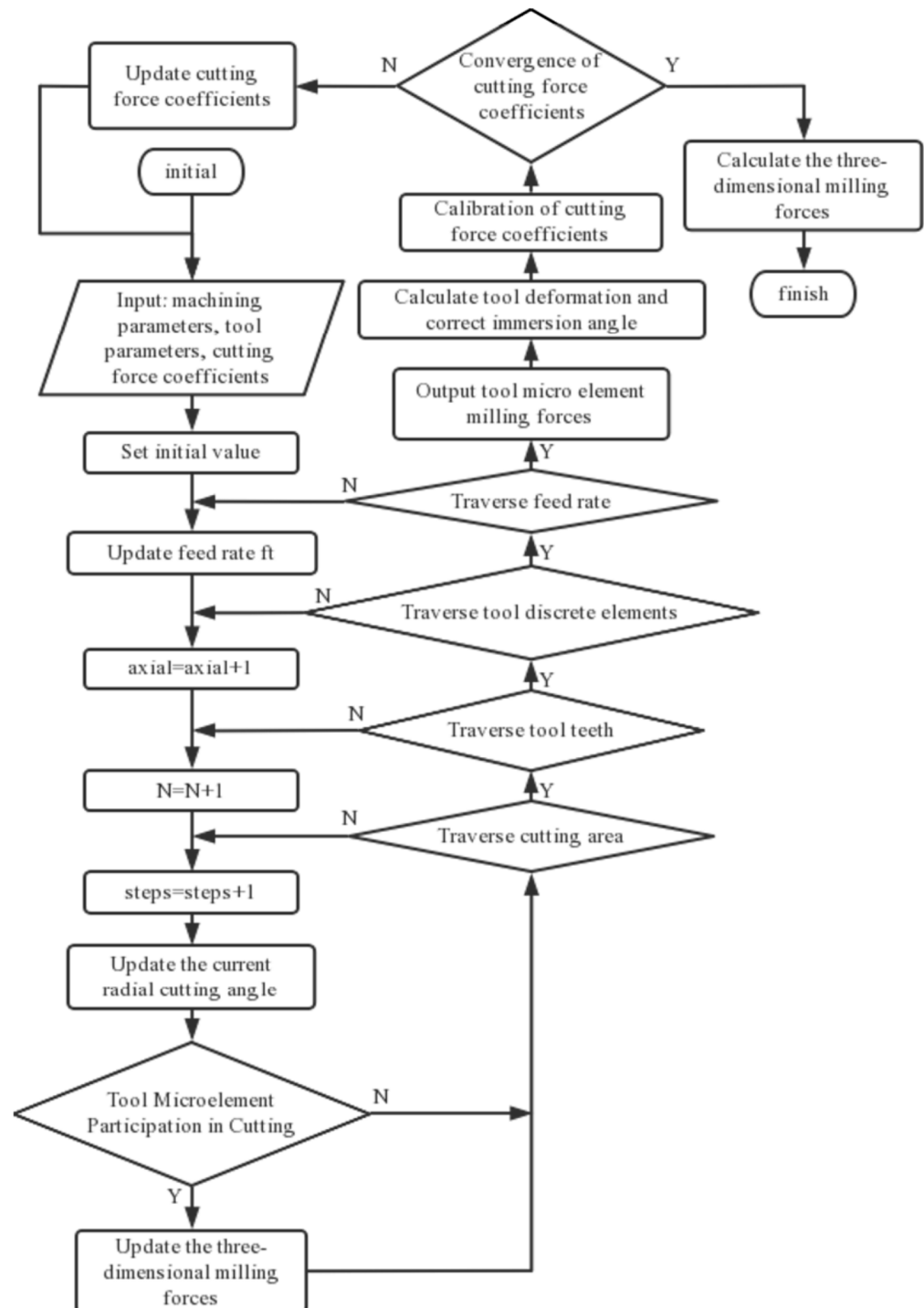


Figure 4. Cutting force coefficients calibration and Cutting force modeling.

The cutting point on the j -th cutting edge of the k -th tool micro-element on the tool is given as P_{kj} . Since the tool has a helix angle, the radial cutting angle of the tool micro-element with different axial heights of the same cutting edge is different, so the cutting angle for the h -th step of the cutting point P_{kj} can be expressed by the following equation:

$$\varphi = \varphi_s + steps_i \times d\varphi + (N_j - 1) \times 360/N - (steps_axial_k - 1) \times db \times \tan(\gamma)/(d/2) \quad (6)$$

According to the mechanical model that was mentioned by Schmitz [16], the three-dimensional forces on the tool micro-element $\{i, j\}$ can be expressed as follows:

$$\begin{cases} F_x = g(\varphi)[F_t \cos(\varphi) + F_n \sin(\varphi)] \\ F_y = g(\varphi)[F_t \sin(\varphi) - F_n \cos(\varphi)] \\ F_z = g(\varphi) \times (-F_a) \end{cases} \quad (7)$$

As peripheral milling is an interrupted cut, the cutting phenomenon only occurs when the knife teeth are in contact with the workpiece, so a window function is introduced in Equation (7) in order to determine whether the micro-element of the cutting edge is involved in the cutting, and its expression is:

$$g(\varphi) = \begin{cases} 1 & \varphi_{s,k} < \varphi < \varphi_{e,k} \\ 0 & \text{others} \end{cases} \quad (8)$$

This corrects the cutting boundary by calculating tool deformation and recalculates the cutting region, where $\varphi_{s,k}$ is the cutting angle of the cutting edge micro-element after correction, and where $\varphi_{e,k}$ is the cutting angle of the cutting edge micro-element after correction.

4. Experimental Verification and Analysis

To verify the method proposed in this paper, cutting experiments should be conducted on a vertical milling machine, as shown in Figure 5. Cutting forces were measured and recorded using a three-component dynamometer KISTLER 9257B. Tool parameters and machining parameters are shown in Tables 2 and 3.

The average values of the milling forces for the stable milling part of the entire milling experiment obtained by the calculation of the dynamometer software are shown in Table 4.

Table 2. Main parameters of the tool.

Diameter d /mm	Number of Teeth N	Tooth Spacing ($^\circ$)	Helix Angle γ ($^\circ$)	Total Length l /mm	Young's Modulus E (GPa)	Clamping Stiffness K_c (N/mm)
12	4	90	30	40	222500	19800

Table 3. Machining Parameter.

Feed Rate f_t /(mm/teeth)	Spindle Speed ω /(r/min)	Radial Depth a /(mm)	Axial Depth b /(mm)
[0.025 0.05 0.075 0.1]	1500	1	4

Table 4. Milling test parameters and average forces measurement results.

b	\bar{F}/N	Feed Rate per Tooth/mm	
		0.075	0.1
4 mm	F_x	95.23	112.7
	F_y	83.28	104.1
	F_z	-25.76	-33.11

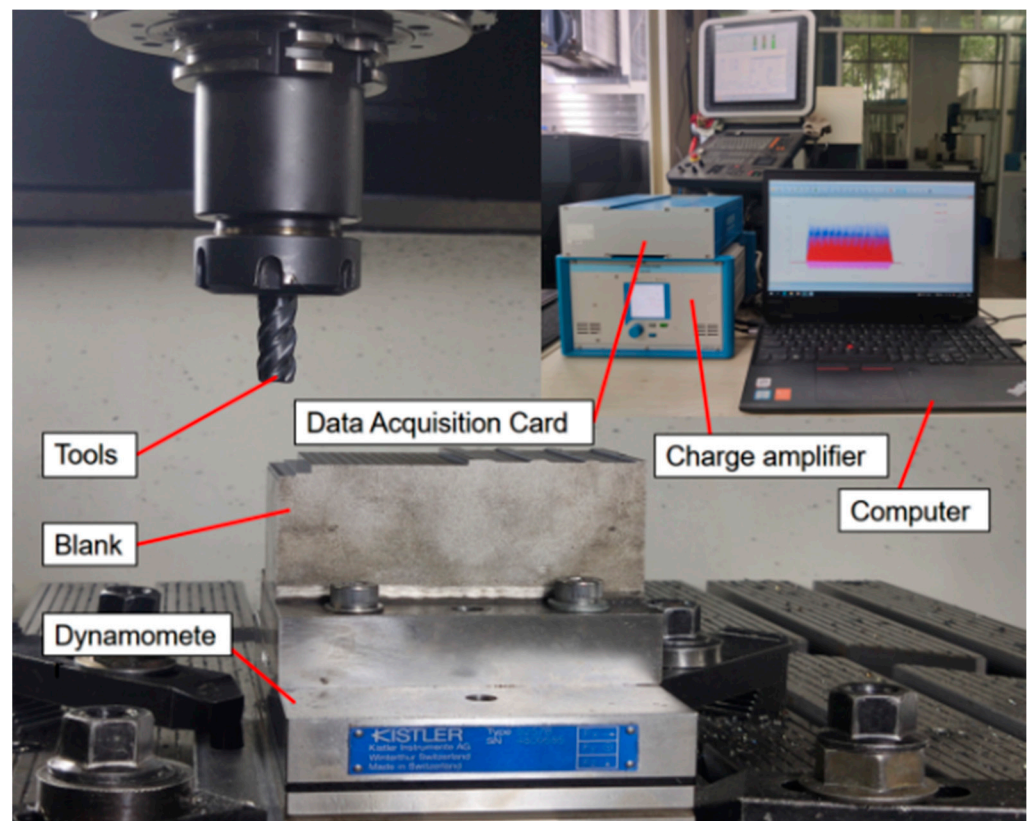


Figure 5. Variable feed peripheral milling experiment.

The cutting force coefficients calibration method introduced in Section 2.1 was used to numerically simulate the milling forces of peripheral milling using Matlab software, and the cutting force coefficients and edge force coefficients were calculated for the two cases on whether tool deformation is considered, as shown in Table 5:

Table 5. Milling force coefficients calibrated by simulation.

b	Tool Deformation	K_{tc}	K_{nc}	K_{ac}	K_{te}	K_{ne}	K_{ae}
4 mm	Yes	2615.94	1144.38	725.044	25.34	6.88	2.08
	No	2568.55	1111.5	710.534	25.11	6.74	2.06

When tool deformation is not considered, the immersion angle is 146.4427° . The simulation model converges to 146.79° after the iterations of the cutting boundary and the cutting force coefficients.

The measured values of the cutting forces for a feed rate of 0.075 mm/tooth and 0.1 mm/tooth are shown in Figure 6. It can be seen from the graph that the fluctuation of the milling forces throughout the milling process is very small, with little change in peak value, and with a stable milling process.

To verify the accuracy of the model, the corresponding cutting parameters were substituted back into the milling forces model in order to obtain predicted milling forces for feed rates of 0.075 mm/tooth and 0.1 mm/tooth. The force signals for a rotation period during the stabilization phase of the experimental data were taken, and the experimental results were compared with the predictions of the model, taking into account the deformation and those without deformation. The three-dimensional milling forces at different feed rates were compared, and the results are shown in Figures 7–9. Comparison results between the average experimental milling force and the average simulated milling force are shown in Table 6.

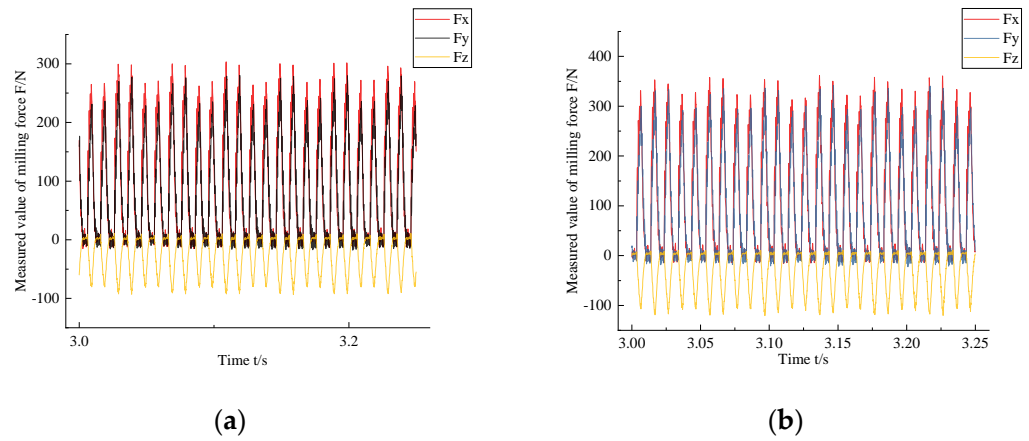


Figure 6. Measured values of different feed rates: (a) feed rate ($f_t = 0.075$ mm/tooth); (b) feed rate ($f_t = 0.1$ mm/tooth).

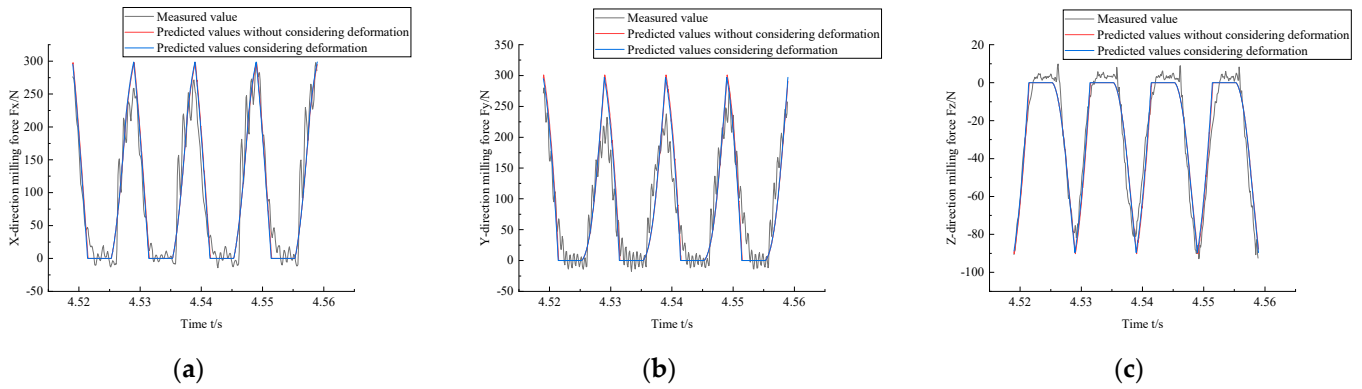


Figure 7. Comparison of predicted and measured milling forces ($f_t = 0.075$ mm/tooth): (a) X-direction milling force; (b) Y-direction milling force; (c) Z-direction milling force.

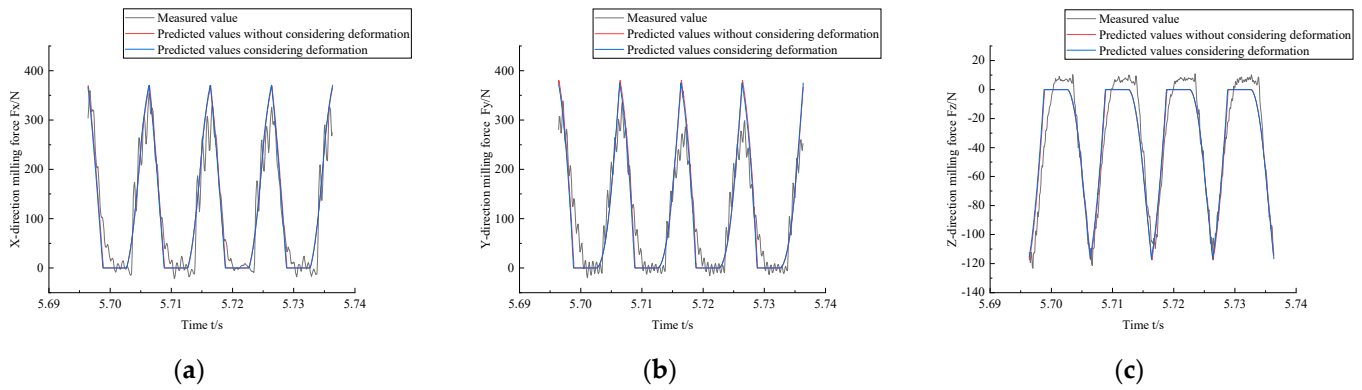


Figure 8. Comparison of predicted and measured milling forces ($f_t = 0.1$ mm/tooth): (a) X-direction milling force; (b) Y-direction milling force; (c) Z-direction milling force.

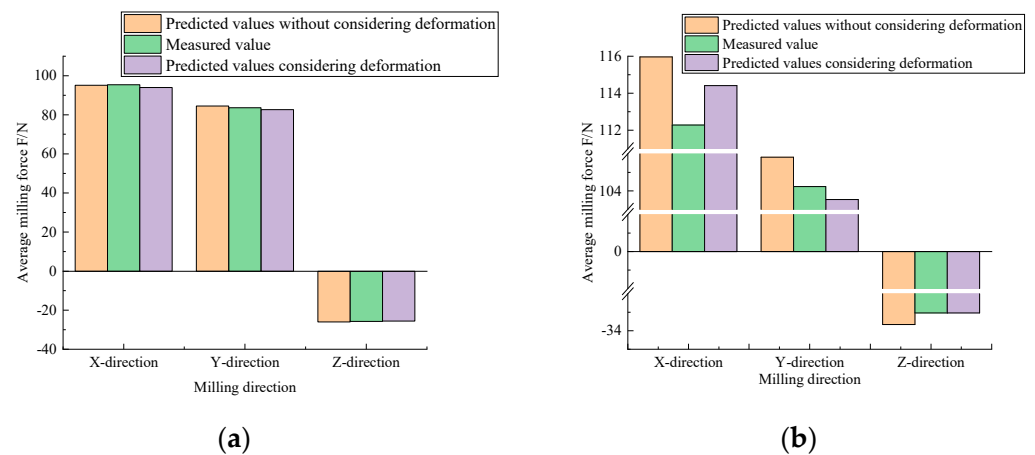


Figure 9. Comparison of the predicted and measured average milling forces: (a) mean milling forces ($f_t = 0.075$ mm/tooth); (b) mean milling forces ($f_t = 0.1$ mm/tooth).

Table 6. Comparison results of experimental and simulated milling force average values.

Feed Rate f_t /(mm/teeth)	\bar{F}/N	Considering Tool Deformation	Measured Value	Without Considering Deformation	Error Reduction Value/%
0.075	F_x	93.93	95.4254	95.166	-1.29
	F_y	82.67	83.6391	84.457	0.12
	F_z	-25.544	-25.7291	-26.03	0.45
0.1	F_x	114.4050	112.2844	115.966	1.4
	F_y	103.53	104.2353	105.82	0.84
	F_z	-33.036	-33.042	-33.67	1.88

The data for a feed rate of 0.075 mm/tooth is shown in Figure 7. The actual tool-cutting region is reduced after considering the tool deformation, which is eventually reflected in the reduction of cutting forces. It can be seen that in the case of small tool deformation, the predicted milling forces in the three directions considering tool deformation are close to the predicted values without considering tool deformation, and since only the radial deformation of the tool is taken into account, the predicted values of milling forces in the Y direction vary more significantly than those in the X and Z directions. As shown in Figure 9a, in the X direction, the predicted mean value without deformation is 95.166 N, the predicted mean value with deformation is 93.93 N, and the measured mean value is 95.4254 N. The error between the predicted and measured values is reduced by -1.29% by taking into account the deformation of the workpiece. In the Y direction, the predicted mean value without deformation is 84.457 N, the predicted mean value with deformation is 82.67 N, and the measured mean value is 83.6391 N. The error between the predicted and the measured values is reduced by 0.12% by taking into account the deformation of the workpiece. In the Z direction, the predicted mean value without deformation is -26.03 N, the predicted mean value with deformation is -25.544 N, and the measured mean value is -25.7291 N. The error between the predicted and the measured values is reduced by 0.45% by taking into account the deformation of the workpiece.

The data for the feed rate of 0.1 mm/tooth are shown in Figure 8, and the results are similar to the data plot for the feed rate of 0.075 mm/tooth. Analysis of Figure 9b shows that in the X direction, the predicted average value without considering deformation is 115.966 N, the predicted average value with considering deformation is 114.405 N, and the measured average value is 112.2844 N. Considering the deformation of the workpiece makes the predicted value and the error between the predicted and the measured values reduce by 1.4%. In the Y direction, the predicted mean value without considering deformation is

105.82 N, the predicted mean value considering deformation is 103.53 N, and the measured mean value is 104.2353 N. The error between the predicted and the measured values is reduced by 0.84% by considering workpiece deformation. In the Z direction, the predicted average value without considering deformation is -33.67 N, the predicted average value considering deformation is -33.036 N, and the measured average value is -33.042 N. The error between the predicted and the measured values is reduced by 1.88% considering workpiece deformation. Compared with the feed rate of 0.075 mm/tooth, the accuracy of the predicted value with the consideration of deformation at the feed rate of 0.1 mm/tooth is improved more.

It is important to know that the method that does not take deformation into account is a calibration method based on the average force of slot milling and is a regression method, which is the same as the one proposed in this paper, and both of the methods are regressions of the measured force. Even though the method without considering the deformation may be as close to the measured value as the proposed method, the coefficients based on that calibration are equivalent to corrections that do not take deformation into account. Moreover, although the method without considering deformation meets the fitting of the cutting force, it does not match the actual proportion of cutting force coefficients, and the calibrated coefficients of the method in this paper are closer to the reality. As shown in Figure 7, although for the individual experimental groups, such as the one in the X direction, the prediction of cutting forces considering deformation are not as good as the results without considering deformation, the cutting force coefficients that are obtained by the proposed method are still closer to the real physical action, and in most of the cases when tool deformation is large, the proposed method is therefore still more advantageous than the other one.

It is worth noting that the tool deformation is very small, with a feed rate of 0.1 mm/tooth and a tool-free end deflection of 0.028 mm. When a slender tool is used, the radial deformation of the tool becomes more pronounced and the prediction of the model becomes more pronounced. The measured milling force is almost consistent with the predicted values in the positions and the waveform trends of the peaks and valleys, which indicates that the prediction ability of the model is good. It should still be noted, though, that there are deviations between the measured and the predicted values because intermittent milling causes unavoidable fluctuations, and the established model does not take into account the influence of factors such as tool run-out and machining chatter in actual machining. As a result, the works that relate to this need to be further studied.

To further investigate the effect of tool parameters on the predicted results of this model, simulation predictions were made for tools with different Young's modulus, and the predicted results are shown in Table 7 below. As Young's modulus of the tool decreases, the tool deformation increases, and the predicted values deviate even more from the experimental values. This shows that it is necessary to consider tool deformation for simulation modeling.

Table 7. Comparison of predicted results for different Young's modulus of tools.

Feed Rate f_t /(mm/teeth)	\bar{F} /N	Measured Value	$E = 222500$ GPa	$E = 150000$ GPa	$E = 100000$ GPa
0.1	F_x	112.2844	114.4050	118.23	119.09
	F_y	104.2353	103.53	109.16	110.44
	F_z	-33.042	-33.036	-34.59	-34.95

5. Conclusions

A peripheral milling forces model that takes into account tool deformation is established in this paper, and a new method for calibrating the cutting force coefficients for end milling is proposed. The calibration accuracy of the cutting force coefficient is im-

proved, and a recalculation of the model machining region is based on the obtained tool deformation in order to further improve the accuracy of cutting force prediction.

Several sets of peripheral milling experiments were conducted, and theoretical analysis was also conducted. The main conclusions are as follows:

(1) Under the consideration of tool deformation, the error of mean milling forces in the X, Y, and Z directions is reduced by -1.29% , 0.12% , and 0.45% , respectively, for a feed rate of 0.075 mm/tooth. The mean errors in the X, Y, and Z directions at a feed rate of 0.1 mm/tooth were reduced by 1.4% , 0.84% , and 1.88% , respectively, which verified the validity of the proposed model. The prediction of the mean milling forces is more accurate at a feed rate of 0.1 mm/tooth, which indicates that the greater the tool deformation during milling, the better the prediction of the model.

(2) This paper creatively calibrates the cutting force coefficients from the perspective of tool deformation, and the calibrated cutting force coefficients are closer to the real values than the traditional calibration method based on the average force of slot milling. In the case of small tool deformation, this method is as close to the measured value as the traditional method. In the case of large tool deformation, the model proposed in this paper predicts the results more accurately in most cases, and is thus the more advantageous method.

Author Contributions: Conceptualization, S.J.; data curation, S.J. and C.Y.; writing—original draft preparation, C.Y., R.Y. and S.J.; writing—review and editing, C.Y., R.Y. and S.J.; supervision, R.Y. and S.J. All authors have read and agreed to the published version of the manuscript.

Funding: This research was funded by the Inner Mongolia Natural Science Foundation (Grant No. 22200-5203168), the National Natural Science Foundation of China (Grant No. 5220053301) and Machining and microstructure testing of high entropy Half-Heusler thermoelectric alloys, 22200-5226035.

Institutional Review Board Statement: Not applicable.

Informed Consent Statement: Not applicable.

Data Availability Statement: Not applicable.

Acknowledgments: Special thanks go to the Key Laboratory of Vehicle Advanced Manufacturing, Measuring, and Control Technology for supporting this work.

Conflicts of Interest: The authors declare that they have no known competing financial interests or personal relationships that could have influenced the work reported in this paper.

Appendix A. Geometric Constants for the Cutter Zones

The geometric constants A , B , and C are defined by Equation (1), which is repeated here for convenience:

$$\begin{aligned} A_1 &= Z \Big|_{Z_1}^{Z_2}, \quad A_2 = \cos \beta \cdot Z \Big|_{Z_1}^{Z_2}, \quad A_3 = \sin \beta \cdot Z \Big|_{Z_1}^{Z_2} \\ B_1 &= \frac{1}{\cos \gamma \cdot \cos \beta} \cdot Z \Big|_{Z_1}^{Z_2}, \quad B_2 = \frac{1}{\cos \gamma} \cdot Z \Big|_{Z_1}^{Z_2}, \quad B_3 = \frac{\tan \beta}{\cos \gamma} \cdot Z \Big|_{Z_1}^{Z_2} \\ C_1 &= \frac{1}{2} \varphi \Big|_{\varphi_s}^{\varphi_e}, \quad C_2 = \frac{1}{4} \sin 2\varphi \Big|_{\varphi_s}^{\varphi_e}, \quad C_3 = \frac{1}{4} \cos 2\varphi \Big|_{\varphi_s}^{\varphi_e}, \quad C_4 = \sin \varphi \Big|_{\varphi_s}^{\varphi_e}, \quad C_5 = \cos \varphi \Big|_{\varphi_s}^{\varphi_e} \end{aligned} \quad (A1)$$

where the integration boundaries Z_1 and Z_2 depend on the immersion of each cutting edge and for cylindrical end mill $\beta = 0$.

References

- Morelli, L.; Grossi, N.; Scippa, A.; Campatelli, G. Extended classification of surface error shapes in peripheral end-milling operations. *J. Manuf. Process.* **2021**, *71*, 604–624. [[CrossRef](#)]
- Yuwen, S.U.N.; Jinjie, J.I.A.; Jinting, X.U.; Mansen, C.H.E.N.; Jinbo, N.I.U. Path, feed rate and trajectory planning for free-form surface machining: A state-of-the-art review. *CJA* **2022**, *35*, 12–29.
- Zhou, J.; Ren, J. Predicting cutting force with unequal division parallel-sided shear zone model for orthogonal cutting. *Int. J. Adv. Manuf. Technol.* **2020**, *107*, 4201–4211. [[CrossRef](#)]

4. Sun, Y.; Jiang, S. Predictive modeling of chatter stability considering force-induced deformation effect in milling thin-walled parts. *Int. J. Mach. Tools Manuf.* **2018**, *135*, 38–52. [[CrossRef](#)]
5. Sun, Y.; Zheng, M.; Jiang, S.; Zhan, D.; Wang, R. A State-of-the-Art Review on Chatter Stability in Machining Thin-Walled Parts. *Machines* **2023**, *11*, 359. [[CrossRef](#)]
6. Szecsi, T. Cutting force modeling using artificial neural networks. *J. Mater. Process. Technol.* **1999**, *93*, 344–349. [[CrossRef](#)]
7. Wang, J.J.; Zheng, C.M. Identification of shearing and ploughing cutting constants from average forces in ball-end milling. *Int. J. Mach. Tools Manuf.* **2002**, *42*, 695–705. [[CrossRef](#)]
8. Budak, E.; Altintas, Y.; Armarego, E. Prediction of Milling Force Coefficients from Orthogonal Cutting Data. *J. Manuf. Sci. Eng. ASME* **1996**, *118*, 216–224. [[CrossRef](#)]
9. Kao, Y.C.; Nguyen, N.T.; Chen, M.S.; Huang, S.C. A combination method of the theory and experiment in the determination of cutting force coefficients in ball-end mill processes. *J. Comput. Des. Eng.* **2015**, *2*, 233–247. [[CrossRef](#)]
10. Wang, M.; Gao, L.; Zheng, Y. An examination of the fundamental mechanics of cutting force coefficients. *Int. J. Mach. Tools Manuf.* **2014**, *78*, 1–7. [[CrossRef](#)]
11. Guo, Q.; Zhao, B.; Jiang, Y.; Zhao, W. Cutting force modeling for non-uniform helix tools based on compensated chip thickness in a five-axis flank milling process. *Precis Eng.* **2018**, *51*, 659–681. [[CrossRef](#)]
12. Kao, Y.C.; Nguyen, N.T.; Chen, M.S.; Su, S.T. A prediction method of cutting force coefficients with a helix angle of flat-end cutter and its application in a virtual three-axis milling simulation system. *Int. J. Adv. Manuf. Technol.* **2015**, *77*, 1793–1809. [[CrossRef](#)]
13. Liu, X.; Gao, H.; Yue, C.; Li, R.; Jiang, N.; Yang, L. Investigation of the milling stability based on modified variable cutting force coefficients. *Int. J. Adv. Manuf. Technol.* **2018**, *96*, 2991–3002. [[CrossRef](#)]
14. Gradišek, J.; Kalveram, M.; Weinert, K. Mechanistic identification of specific force coefficients for a general end mill. *Int. J. Mach. Tools Manuf.* **2004**, *44*, 401–414. [[CrossRef](#)]
15. Budak, E.; Altintas, Y. Modeling and avoidance of static form errors in peripheral milling of plates. *Int. J. Mach. Tools Manuf.* **1995**, *35*, 459–476. [[CrossRef](#)]
16. Schmitz, T.L.; Smith, K.S. *Machining Dynamics*; Springer: Berlin/Heidelberg, Germany, 2009; p. 303.

Disclaimer/Publisher’s Note: The statements, opinions and data contained in all publications are solely those of the individual author(s) and contributor(s) and not of MDPI and/or the editor(s). MDPI and/or the editor(s) disclaim responsibility for any injury to people or property resulting from any ideas, methods, instructions or products referred to in the content.